Characterization and generation of a SQL-beating cat-like state through repetitive measurements

Mamiko Tatsuta,^{1,*} Yuichiro Matsuzaki,^{1,†} Hiroki Kuji,^{1,2,‡} Ryusuke Hamazaki,^{3,4,§} and Akira Shimizu^{5,6,¶}

¹Department of Electrical, Electronic, and Communication Engineering,
Faculty of Science and Engineering, Chuo university, 1-13-27, Kasuga, Bunkyo-ku, Tokyo 112-8551, Japan
²Department of Physics, Tokyo University of Science, 1-3 Kagurazaka, Shinjuku, Tokyo, 162-8601, Japan
³Nonequilibrium Quantum Statistical Mechanics RIKEN Hakubi Research Team,
RIKEN Pioneering Research Institute (PRI), Wako, Saitama 351-0198, Japan
⁴RIKEN Center for Interdisciplinary Theoretical and Mathematical Sciences (iTHEMS), RIKEN, Wako 351-0198, Japan
⁵Institute for Photon Science and Technology, The University of Tokyo, 7-3-1 Hongo, Bunkyo-ku, Tokyo 113-0033, Japan
⁶Center for Quantum Information and Quantum Biology,
The University of Osaka, Toyonaka, Osaka 560-0043, Japan
(Dated: August 26, 2025)

Sensitivity in metrology without entanglement is limited by standard quantum limit (SQL). Recent studies have found that the Heisenberg-limited scaling – ultimate sensitivity in quantum metrology – can be achieved by generalized cat states, characterized by an index that indicates coherence among macroscopically distinct states. Although generalized cat states include diverse states, encompassing classical mixtures of exponentially large numbers of states, the preparation of large generalized cat states has not been demonstrated yet. Here, we characterize SQL-beating cat-like states using the index q indicating macroscopic coherence and prove that any state with q>1.5 has a potential to surpass the SQL when used as a sensor. We then propose a protocol to generate them through repetitive measurements on a quantum spin system of N spins, which we call a spin ensemble. Starting from a thermal equilibrium state of the spin ensemble, we demonstrate that we can increase the coherence among the spin ensemble via repetitive weak measurements of its total magnetization, which is indirectly measured through an ancillary qubit collectively coupled to the ensemble. Notably, our method for creating the SQL-beating cat-like states requires no dynamical control over the spin ensemble. As a potential experimental realization, we discuss a hybrid system composed of a superconducting flux qubit and donor spins in silicon. Our results pave the way for the realization of entanglement-enhanced quantum metrology in state-of-the-art technology.

I. INTRODUCTION

High-precision measurement is of paramount importance in both fundamental research and applied science [1-4]. Numerous critical parameters, including temperature, electric field, and pressure, require precise measurement. In particular, magnetic field sensing has garnered considerable attention [5– 7], serving not only to investigate material properties but also to elucidate biological mechanisms. Substantial efforts have been devoted to enhancing the sensitivity of magnetic field sensors [8–25]. One promising approach to improving sensitivity is the utilization of qubits [26–34]. Magnetic fields induce shifts in the resonant frequency of qubits, allowing the estimation of magnetic field strength via Ramsey-type measurements. When employing N qubits in separable states, the uncertainty (i.e., the reciprocal of sensitivity) scales as $N^{-1/2}$, which is called the standard quantum limit (SQL). Conversely, using a specific type of entangled state, the sensitivity scales as N^{-1} , achieving what is known as the Heisenberg-limited scaling. In realistic scenarios, environmental decoherence cannot be avoided [9, 11, 19, 22, 23, 25, 35-40], making it challenging to reach the Heisenberg-limited scaling. Nevertheless, it is established that under certain conditions of decoherence, it is possible to surpass the SQL in scaling. For instance, in the presence of time-inhomogeneous dephasing, the uncertainty scales as $N^{-3/4}$, referred to as the Zeno limit [9, 41].

The concept of superposition involving macroscopically distinct states has been a topic of fundamental interest since its inception by Schrödinger [42]. The Greenberger-Horne-Zeilinger (GHZ) [43–45] state is a quintessential example of such a superposition. The GHZ state is expressed as $(|\uparrow\rangle^{\otimes N} + |\downarrow\rangle^{\otimes N})/\sqrt{2}$, where $|\uparrow\rangle$ and $|\downarrow\rangle$ are eigenstates of the Pauli operator $\hat{\sigma}_3$ with eigenvalues +1 and -1, respectively. Despite numerous studies, a unified criterion to determine whether a given state contains such macroscopic superpositions remains elusive [46].

Among the various potential metrics, an "index q" [47], a real number satisfying $1 \le q \le 2$, is particularly noteworthy for gaining deeper insights into the correlation between cat states and sensor technologies. A state with q=2 is referred to as a generalized cat state. Notably, there exists a generalized cat state $\hat{\rho}_m$ with exponentially small purity, i.e., $\mathrm{Tr}(\hat{\rho}_m^2) = \exp(-\Theta(N))$ [48]. It has been shown that utilizing generalized cat states for magnetic field sensing can achieve the Heisenberg-limited scaling in the absence of decoherence [49] and the Zeno limit in the presence of time-inhomogeneous dephasing [9, 41]. Thus, generalized cat states present a compelling metrological approach, leveraging quantum properties to significantly enhance sensitivity.

A theoretical proposal exists for the creation of a generalized cat state [50]. By commencing with a thermal equilibrium state of a quantum spin system of N spins, which we

^{*} email address:mamikotatsuta@gmail.com

[†] email address: ymatsuzaki872@g.chuo-u.ac.jp

[‡] email address:1225702@ed.tus.ac.jp

[§] email address:ryusuke.hamazaki@riken.jp

[¶] email address:shmz@as.c.u-tokyo.ac.jp

call a spin ensemble, it is possible to generate the generalized cat state [50], by performing high-resolution, in this case $\Theta(1)$, measurement of magnetization. However, current technology does not allow such a high-resolution measurement of the magnetization of a spin ensemble. Consequently, a more accessible method for creating a large generalized cat state remains elusive.

In this study, we first use the index q to characterize states that are advantageous for quantum sensing, i.e., beating the SQL although less sensitive than generalized cat states. We call such states, which satisfy 1.5 < q < 2, the SQL-beating cat-like states. We then propose a method to create such SQL-beating states from a thermal equilibrium state of a spin ensemble through repetitive low-resolution measurements of the total magnetization, utilizing an ancillary qubit coupled with the spin ensemble. We prove that we obtain a SQL-beating cat-like state with probability 1 in the large N limit. We also perform numerical simulations to observe gradual emergence of such a state.

This paper is outlined as follows. In Sec. II, we review three important notions: the definition of the index q, a recipe to create a generalized cat state via single projective measurement, and basics of quantum metrology. Section III discusses our finding on the relation between the sensitivity and the value of q, especially when 1.5 < q < 2. In Sec. IV, we propose a protocol to create a SQL-beating cat-like state via repetitive measurements, especially within a spin ensemble in a solid state system read out by a superconducting qubit. In Sec. V we analyze the final state of the spin ensemble after measurements and clarify the condition of successfully generating a generalized cat state. We also discuss the success probability and evaluate how many measurements are required to approximately obtain the state we want. Numerical simulations are given in Sec. VI, and we indeed observe the emergence of SQL-beating cat-like states. Section VII concludes the manuscript.

II. PRELIMINARIES

We first review the previous works on generalized cat states and a way of obtaining them from thermal equilibrium states through a single measurement. We also review Ramsey-type quantum metrology using highly entangled states. Throughout this paper, we take $\hbar=1$.

A. Generalized cat states

First, let us briefly review the concept of generalized cat states, characterized by an index denoted as q [51]. For a comprehensive discussion, refer to Ref. [52].

The index q is utilized to detect macroscopic coherence in a given quantum state $\hat{\rho}$, which may be pure or mixed. It is defined through the following relation:

$$\max \left\{ \max_{\hat{A}} \frac{1}{2} \| [\hat{A}, [\hat{A}, \hat{\rho}]] \|_{1}, N \right\} = \Theta(N^{q}), \tag{1}$$

where $\|\hat{X}\|_1 = \text{Tr}\sqrt{\hat{X}^\dagger\hat{X}}$ is the trace norm, \hat{A} is an additive observable, defined as $\hat{A} = \sum_{l=1}^N \hat{a}(l)$ with $\hat{a}(l)$ acting on a single spin at site l [53]. By definition, the index satisfies the condition of $1 \le q \le 2$. The trace norm can be expressed as

$$\frac{1}{2} \| [\hat{A}, [\hat{A}, \hat{\rho}]] \|_1 = \max_{\hat{\eta}} \operatorname{Tr} \left(\hat{\eta} [\hat{A}, [\hat{A}, \hat{\rho}]] \right) \tag{2}$$

$$= \max_{\hat{\eta}} \sum_{A,A',\nu,\nu'} (A - A')^2 \langle A, \nu | \hat{\rho} | A', \nu' \rangle \langle A', \nu' | \hat{\eta} | A, \nu \rangle,$$
(3)

where A ($|A,\nu\rangle$) are eigenvalues (eigenstates) of \hat{A} , i.e., $\hat{A} |A,\nu\rangle = A |A,\nu\rangle$, with ν labeling the degeneracy, and $\hat{\eta}$ is a projection operator, which satisfies $\hat{\eta}^2 = \hat{\eta}$. From this expression, we find that $\frac{1}{2} \|[\hat{A},[\hat{A},\hat{\rho}]]\|_1$ indicates macroscopic coherence between two macroscopically distinct states, and that q can be interpreted as a measure to quantify how close the state is to the cat state. For example, it is evident that macroscopic coherence, i.e., $\langle A,\nu|\hat{\rho}|A',\nu'\rangle$ with $|A-A'|=\Theta(N)$ [or $(A-A')^2=\Theta(N^2)$], has a substantial weight in the trace norm of the double commutator if the state has q=2. Then, we can conclude that a state $\hat{\rho}$ with q=2 contains a substantial amount of superposition of macroscopically distinct states.

In addition to the index q, we introduce a term "a generalized cat state." We call $\hat{\rho}$ a generalized cat state of \hat{A} if there exists a projection operator $\hat{\eta}$ such that

$$Tr(\hat{\eta}[\hat{A}, [\hat{A}, \hat{\rho}]]) = \Theta(N^2) \tag{4}$$

for a given \hat{A} . From this definition, a generalized cat state has q=2. Conversely, each state with q=2 is regarded as a generalized cat state of some observable \hat{A} . As detailed in Sec. II C, generalized cat state exhibits a significant quantum advantage when used in metrology.

B. From a thermal equilibrium state to a generalized cat state

In this subsection, we review a protocol to obtain a generalized cat state from a thermal equilibrium state of a spin ensemble using high-resolution measurements. We define $\hat{S}_{\alpha} = \sum_{i=1}^{N} \hat{\sigma}_{\alpha}(i)$ with $\alpha = x,y,z$, where $\hat{\sigma}_{\alpha}$ denotes a Pauli operator.

In [50], it was proven that a single ideal measurement of the total magnetization can transform a thermal equilibrium state into a generalized cat state. This protocol involves the following steps:

1. Prepare the spins in a thermal equilibrium state in a magnetic field along the z-axis, represented by h, at a temperature $1/\beta$. The Hamiltonian is $\hat{H}_P = -\omega_P \hat{S}_z$, where $\omega_P = h$. The initial state is then given by $\hat{\rho}_P = e^{\beta\omega_P \hat{S}_z}/Z_P$, where $Z_P = \text{Tr}(e^{\beta\omega_P \hat{S}_z})$. Here, the subscript P stands for the phosphorus donor electrons, which we consider as a spin ensemble to generate generalized cat states in Sec. IV A.

2. Perform a projection measurement onto the $\hat{S}_x = M$ subspace. The post-measurement state is expressed as $\hat{\rho}_{\mathrm{PM}} = \hat{\mathcal{P}}(M)e^{\beta\omega_{\mathrm{P}}\hat{S}_z}\hat{\mathcal{P}}(M)/Z_{\mathrm{PM}}$, where $\hat{\mathcal{P}}(M)$ denotes the projection onto the $\hat{S}_x = M$ subspace, and $Z_{\mathrm{PM}} = \mathrm{Tr}(\hat{\mathcal{P}}(M)e^{\beta\omega_{\mathrm{P}}\hat{S}_z})$.

It can be shown that

$$\operatorname{Tr}(\hat{\mathcal{P}}(M)[\hat{S}_z, [\hat{S}_z, \hat{\rho}_{PM}]]) = (N^2 - M^2) \tanh^2(\beta \omega_P) + 2N,$$
(5)

indicating that $\hat{\rho}_{\mathrm{PM}}$ is a generalized cat state of \hat{S}_z when $\beta\omega_{\mathrm{P}}=\Theta(N^0)>0$ and $M\neq \pm N+o(N).$ Note that this value may be smaller than $\frac{1}{2}\|[\hat{S}_z,[\hat{S}_z,\hat{\rho}_{\mathrm{PM}}]]\|_1$, since taking the trace norm $\|\hat{X}\|_1$ of Hermitian \hat{X} corresponds to applying a projection operator $\hat{\eta}_M$ that maximizes $2\mathrm{Tr}(\hat{\eta}_M\hat{X}).$ Interestingly, for finite temperature $1/\beta,$ this generalized cat state exhibits an exponentially small purity, i.e., $\mathrm{Tr}(\hat{\rho}_{\mathrm{PM}}^2)\leq \exp(-\Theta(N))$, due to the highly mixed nature of the premeasurement Gibbs state. This explanation pertains to a simple case with no interactions between spins. However, it was also proven in [50] that a generalized cat state of \hat{S}_z can be obtained even in the presence of interaction between the spins.

A significant challenge of this scheme lies in the requirement for high-resolution measurements. If the precision of the projection $\hat{\mathcal{P}}(M)$, equivalent to the minimum resolvable number of spins, is $\Theta(\sqrt{N})$, the conversion to a generalized cat state occurs with a probability of $\exp(-\Theta(N))$. To achieve a generalized cat state with a probability that remains constant as N increases, the projection $\hat{\mathcal{P}}(M)$ must be performed with a precision of $\Theta(1)$. This level of precision is experimentally demanding with a single readout. In this paper we propose to overcome this difficulty by introducing repetitive measurements.

C. Ramsey-type quantum metrology

Next, let us briefly review Ramsey-type quantum metrology [4] and elucidate how we can utilize our highly entangled state. We adopt this as the basic strategy in our new protocol. Assume that the Hamiltonian describing the interaction with the magnetic field is $\hat{H} = -\omega \hat{S}_z$. In a Ramsey-type measurement protocol, a sensor state $\hat{\rho}$ is exposed to the target field for a time $t_{\rm int}$, resulting in the state evolution:

$$\hat{\rho}(t_{\rm int}) = e^{i\omega t_{\rm int}\hat{S}_z} \hat{\rho} e^{-i\omega t_{\rm int}\hat{S}_z}.$$
 (6)

Then a projective measurement is performed. This projection operator can be chosen to optimize the sensitivity. The probability P of the projection $\hat{\eta}$ is given by

$$P = \text{Tr}(\hat{\eta}\hat{\rho}(t_{\text{int}})). \tag{7}$$

This protocol is repeated $T/t_{\rm int}\gg 1$ times, where T is the total measurement time. Here, we assume that the state preparation and readout times are negligible compared to $t_{\rm int}$. From

the measurement outcomes, the parameter ω can be estimated with an uncertainty [49]:

$$\delta\omega = \frac{\sqrt{P(1-P)}}{\left|\frac{dP}{d\omega}\right|} \frac{1}{\sqrt{T/t_{\rm int}}}.$$
 (8)

The inverse of the uncertainty defines the sensitivity. If the initial state is separable (for which q=1), then

$$\delta\omega = \Theta(N^{-1/2}),\tag{9}$$

which is known as the standard quantum limit (SQL). Conversely, a state with q=2 provides us with

$$\delta\omega = \Theta(N^{-1}),\tag{10}$$

which is referred to as the Heisenberg-limited scaling [49]. This enhancement of sensitivity in scaling is crucial in quantum advantage.

The generalized cat state of \hat{A} can be employed to estimate a parameter ω coupled to \hat{A} , where the state evolves under an interaction Hamiltonian $\hat{H}=\omega\hat{A}$. It has been demonstrated that the target parameter ω in this setup can be estimated at the ultimate scaling sensitivity: the Heisenberg-limited scaling $\delta\omega=\Theta(N^{-1})$ in the absence of noise, and the Zeno limit $\delta\omega=\Theta(N^{-3/4})$ in the presence of time-inhomogeneous dephasing [52]. Additionally, the method in [52] provides a detailed prescription of how to achieve this sensitivity using the generalized cat states. That is, the Ramsey-type protocol is utilized, where the generalized cat state is prepared as a probe state, exposed to the target field, and subsequently measured by the projection $\hat{\eta}$.

It is important to note that the quantum Fisher information (QFI) offers the highest sensitivity attainable with a given state via the Cramer-Rao bound [8], assuming an optimal positive operator-valued measure (POVM) is chosen. However, finding the optimal POVM is a core mission in quantum metrology [54] and its physical implementation may be non-trivial. In contrast, the approach using the generalized cat state as proposed in [52] is advantageous because it demonstrates practical experimental implementation. Furthermore, we here introduce a feasible procedure to obtain states with high q value, and explore their features both analytically and numerically.

In the following section, we discuss a novel relation between index q and quantum advantage, generalizing the above relations.

III. SQL-BEATING CAT-LIKE STATES

Given the preliminaries discussed above, we now show our first important result that states with q>1.5 can serve as sensors surpassing the SQL. Specifically, we show that

$$\delta\omega \le 1/\Theta(N^{q-1}). \tag{11}$$

That is, the sensitivity beyond the SQL is achievable for q > 1.5.

Let $\hat{\eta}$ be the projection operator that satisfies the following:

$$\frac{1}{2} \|[\hat{S}_z, \hat{\rho}]\|_1 = \operatorname{Tr}\left(\hat{\eta}[\hat{S}_z, \hat{\rho}]\right). \tag{12}$$

We then obtain the following inequality:

$$\frac{1}{2} \| [\hat{S}_z, [\hat{S}_z, \hat{\rho}]] \|_1 \le 2N \frac{1}{2} \| [\hat{S}_z, \hat{\rho}] \|_1 = 2N |\text{Tr}(\hat{\eta}[\hat{S}_z, \hat{\rho}])|.$$
(13)

This inequality implies that if $\hat{\rho}$ is a generalized cat state of \hat{S}_z , then $\|[\hat{S}_z, \hat{\rho}]\|_1 = \Theta(N)$.

Using the Baker-Hausdorff formula, we have:

$$\hat{\rho}(t) = \sum_{k=0}^{\infty} \frac{(i\omega t)^k}{k!} [\hat{S}_z, \hat{\rho}]_k, \tag{14}$$

where we define $[\hat{S}_z,\hat{\rho}]_0=\hat{\rho}$ and $[\hat{S}_z,\hat{\rho}]_k=[\hat{S}_z,[\hat{S}_z,\hat{\rho}]_{k-1}].$ Hence, we have

$$\left| \frac{dP}{d\omega} \right| = \left| \operatorname{Tr} \left(\hat{\eta} \sum_{k=1}^{\infty} \frac{-i t_{\operatorname{int}} (i\omega t_{\operatorname{int}})^{k-1}}{(k-1)!} [\hat{S}_z, \hat{\rho}]_k \right) \right| \tag{15}$$

$$\simeq \left| \operatorname{Tr} \left(\hat{\eta}(-it_{\text{int}}) [\hat{S}_z, \hat{\rho}] \right) \right| \quad (\omega t_{\text{int}} N \ll 1) \quad (16)$$

$$= t_{\rm int} \left| \text{Tr} \left(\hat{\eta} [\hat{S}_z, \hat{\rho}] \right) \right|, \tag{17}$$

where we have used $\omega t_{\rm int} N \ll 1$, which is a common assumption in quantum metrology.

Therefore, we obtain the following inequality that ensures the advantage of states with q > 1.5:

$$\delta\omega \simeq \frac{\sqrt{P(1-P)}}{|t_{\rm int} {\rm Tr}(\hat{\eta}[\hat{S}_z, \hat{\rho}])|} \frac{1}{\sqrt{T/t_{\rm int}}}$$
(18)

$$\leq \frac{1/2}{\frac{1}{2} \|[\hat{S}_z, \hat{\rho}]\|_1} \frac{1}{\sqrt{Tt_{\text{int}}}} \tag{19}$$

$$\leq \frac{N}{\frac{1}{2} \|[\hat{S}_z, [\hat{S}_z, \hat{\rho}]]\|_1} \frac{1}{\sqrt{Tt_{\text{int}}}}$$
 (20)

$$=\frac{1}{\Theta(N^{q-1})}\frac{1}{\sqrt{Tt_{\rm int}}},\tag{21}$$

which gives (11).

This bound is loose when considering separable states, as they provide a scaling of $\delta\omega=\Theta(N^{-1/2})$, while this bound gives $\delta\omega\leq\Theta(N^0)$. However, this bound is significant for states with q>1.5, because they surpass the SQL in scaling. Therefore, not only the states with q=2 but also states with 1.5< q<2 are advantageous for quantum metrology. We refer to such states as SQL-beating cat-like states and illustrate its emergence as the result of repetitive measurements.

Note that the inequality (18) provides us with the upper bound of $\delta\omega$, while Cramer-Rao bound provides the lower bound. That is, the actual value of uncertainty might be better than what we calculate through our inequality, while the Cramer-Rao bound indicates the lowest limit that might be difficult to achieve because of imperpection of realistic setup.

IV. SETUP OF EMERGENCE OF SQL-BEATING CAT-LIKE STATES VIA REPETITIVE MEASUREMENTS.

We present our protocol for generating SQL-beating catlike states through repetitive measurements. The procedure involves coupling an ancillary qubit with a spin ensemble and subsequently reading out the total magnetization of the spins via the projective measurement of the ancillary qubit. Given that a single measurement of the ancillary qubit yields a binary result, it does not provide direct information on the total magnetization of the spins. However, we demonstrate that through repeated measurements, the thermal equilibrium state is converted into SOL-beating cat-like states due to measurement backaction. Although this scheme can be implemented in various physical systems, we primarily focus on a hybrid system consisting of a superconducting flux qubit (FO) and an electron spin ensemble. Our approach aims to generate generalized cat states within the electron spin ensembles by measuring the spin magnetization with the FQ. In the following, we briefly review each system and subsequently propose our scheme.

A. Spin ensemble

First, we introduce a spin ensemble that we convert into generalized cat states. Specifically, we consider phosphorus (P) donor electrons in a pure 28 Si substrate [55]. We assume that the temperature is low so that all donor electrons are trapped by the donors. The P donor electron possesses a spin of 1/2. The donors are distributed randomly in the substrate, and we assume that the donor density is low, typically 10^{15} cm⁻³ [55], so that spin-spin interactions are negligible. Notably, these spins exhibit a long coherence time of around 10 seconds [55], making them ideal for the creation and manipulation of superposition of macroscopically distinct states.

By applying a magnetic field h along the z axis, the two energy levels are split by the Zeeman energy. The Hamiltonian is described as follows:

$$\hat{H}_{P} = -\omega_{P} \sum_{j=1}^{N} \hat{\sigma}_{z}(j) =: -\omega_{P} \hat{S}_{z}, \qquad (22)$$

where $\omega_P = h$. This ω_P is $\Theta(1)$ and known, unlike the target parameter ω in Sec. II C. The spin ensemble is initially prepared in the canonical Gibbs state with the inverse temperature β [56],

$$\hat{\rho}_{\mathrm{P}}(0) = e^{-\beta \hat{H}_{\mathrm{P}}} / \mathrm{Tr}(e^{-\beta \hat{H}_{\mathrm{P}}}), \tag{23}$$

which has the total spin $\langle \hat{S}_z \rangle = \Theta(N)$ parallel to h. We will manipulate this state by measuring \hat{S}_x , the total spin component perpendicular to h, with the superconducting flux qubit, which we review in the next subsection.

B. Superconducting flux qubit

A superconducting flux qubit (FQ) is an artificial two-level system [57–60]. The FQ comprises a superconducting loop with several (typically three) Josephson junctions, operating at temperatures in the tens of millikelvin. Within the loop, a persistent current I_q flows either clockwise or counterclockwise. The clockwise current corresponds to a state $|R\rangle$, while the counterclockwise current corresponds to the state $|L\rangle$. By defining $\hat{\Sigma}_3 := |R\rangle \langle R| - |L\rangle \langle L|$ and $\hat{\Sigma}_1 := |R\rangle \langle L| + |L\rangle \langle R|$, the Hamiltonian of the FQ can be expressed as follows:

$$\hat{H}_{FQ} = \epsilon \hat{\Sigma}_3 + \Delta \hat{\Sigma}_1 \simeq \epsilon \hat{\Sigma}_3, \tag{24}$$

where $\epsilon=2I_q(\Phi-\Phi_0/2)$ is an energy bias, with Φ representing the magnetic flux penetrating the loop of the FQ, and Φ_0 denoting a flux quantum. Also, Δ is the tunneling energy, and we assume $\Delta\ll\epsilon$. Although Δ is small, it controls the persistent current of the flux qubit [61–63], and will therefore play a crucial role in our scheme. We will take its effect into account whenever necessary, while otherwise we approximate $\hat{H}_{\rm FQ}$ as $\epsilon\hat{\Sigma}_3$.

A flux qubit can be utilized as a sensitive magnetometer for detecting the penetrating magnetic flux Φ [29, 64–67]. To estimate ϵ , which directly translates to estimating the external flux Φ , the following procedure is employed. First, the flux qubit is prepared in the state

$$|+\rangle := (|R\rangle + |L\rangle)/\sqrt{2}.$$
 (25)

This state can be prepared by applying a $\pi/2$ pulse of a resonant microwave [68], a step referred to as initialization. By exposing this state to the target external magnetic field corresponding to ϵ for a duration t, one obtains $(e^{-i\epsilon t}|R\rangle + |L\rangle)/\sqrt{2}$. For readout, we perform a single-qubit rotation using a microwave pulse, followed by measurement using a Josephson bifurcation amplifier [69, 70] or a dispersive readout with a Josephson parametric amplifier. This process corresponds to a projective measurement in the $\hat{\Sigma}_2 := i|L\rangle\langle R| - i|R\rangle\langle L|$, basis.

Each measurement yields either +1 or -1 from the readout apparatus of the FQ, with a probability $P=\cos^2(\epsilon t/2)$ for +1 and $1-P=\sin^2(\epsilon t/2)$ for (-1). By repeating this procedure, we can accurately estimate P, thereby reducing the uncertainty in the estimation of ϵ . According to the central limit theorem, the uncertainty $\delta\epsilon$ depends on the square root of the number of repetitions m:

$$\delta\epsilon \propto \frac{1}{\sqrt{m}}.$$
 (26)

In this paper, we increase m of repetitive measurements with a FQ to convert a thermal equilibrium state into a generalized cat state.

C. Hybrid system

We now introduce the hybrid system comprising N electron spins and a FQ [71–75], where the FQ serves as an ancillary

qubit to repetitively measure the total magnetization of the spin ensemble.

As illustrated in Fig. 1, an ensemble of donor electron spins in silicon is placed inside the loop of the FQ. We apply a magnetic field parallel to the plane of the FQ loop corresponding to the application of $\omega_{\rm P} \hat{S}_z$ as described in Sec. II B. We assume that the spin ensemble's x axis is orthogonal to the plane of the loop. The FQ has two basis states corresponding to the clockwise and counterclockwise currents. These currents generate magnetic fields that shift the Zeeman energy of the electron spin along the x direction. This state-dependent energy shift induces a magnetic interaction between electron spins and the FQ, described by the interaction Hamiltonian:

$$\hat{H}_{\rm int} = g(t)\hat{S}_x \otimes \hat{\Sigma}_3,\tag{27}$$

where g(t) denotes the coupling strength between them.

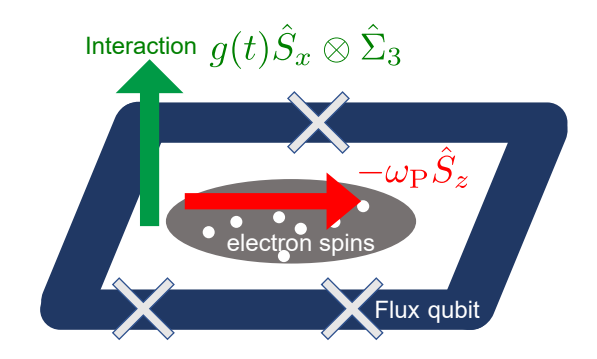


FIG. 1. Schematic of the spin ensemble and the FQ. The electron spins (white dots) are situated on the substrate (gray oval), which is placed within the loop of the FQ (navy parallelogram). An external magnetic field (red arrow) is applied along the z axis to induce the Zeeman energy $-\omega_P \hat{S}_z$. Interaction between the spin ensemble and the FQ is represented by a green arrow.

The total Hamiltonian of the system is

$$\hat{H} = \hat{H}_{FO} + \hat{H}_{P} + \hat{H}_{int}. \tag{28}$$

If the interaction induces a frequency shift on the FQ, we can use the FQ to detect the magnetization of the spin ensemble by performing the Ramsey-type measurements on the FQ. We take $h=\omega_{\rm P}$ large enough such that

$$|g(t)| \ll \omega_{\rm P}$$
 (29)

is satisfied. Under this condition, a DC (time-independent) term in g(t) is unimportant because it will be dropped due to a rotating wave approximation. By contrast, an AC (time-dependent) term in g(t) can induce significant resonant effects if its frequency $\simeq \omega_{\rm P}$. Therefore, we consider the following time-dependent coupling:

$$g(t) = g\cos(2\omega_{\rm P}t) = g\frac{e^{2i\omega_{\rm P}t} + e^{-2i\omega_{\rm P}t}}{2}.$$
 (30)

We can achieve such modulation of the coupling strength by altering the tunneling energy Δ of the FQ since the persistent current of the FQ depends on the tunneling energy [63].

Alternatively, with a time-independent coupling strength, we could perform many π pulses on the FQ sequentially, akin to dynamical decoupling [68], causing the effective coupling strength to oscillate temporarily. In this paper, we focus on the former strategy.

Because of Eqs. (29) and (30), the rotating-wave approximation works well. In the rotating frame defined by $\hat{V} = \exp(-i\omega_{\rm P}t\hat{S}_z + i\epsilon\hat{\Sigma}_3 t)$, we have:

$$\hat{H}_R = \hat{V}\hat{H}\hat{V}^{\dagger} - i\hat{V}\frac{d\hat{V}^{\dagger}}{dt} \tag{31}$$

$$= g(t) \frac{\hat{S}_{+} e^{-2i\omega_{\rm P}t} + \hat{S}_{-} e^{2i\omega_{\rm P}t}}{2} \otimes \hat{\Sigma}_{3}, \qquad (32)$$

where we use $\hat{S}_x=(\hat{S}_++\hat{S}_-)/2$. Thus, the Hamiltonian in the rotating frame becomes

$$\hat{H}_R \simeq \frac{g}{2} \hat{S}_x \otimes \hat{\Sigma}_3. \tag{33}$$

This Hamiltonian indicates that the spin magnetization along the x axis induces a frequency shift on the FQ, allowing us to use Ramsey measurements on the FQ to detect the spin ensembles. Importantly, in this scenario, we do not need to control the spin ensemble with microwave pulses.

As depicted in Fig. 2, we assume that g(t)=0 during the initialization and readout of the FQ, whereas it oscillates as Eq. (30) during interaction. Even if the coupling strength has a DC component, we can ignore its effect, as mentioned above. Below we analyze how the state of the spin ensemble changes by repeating these Ramsey measurements.

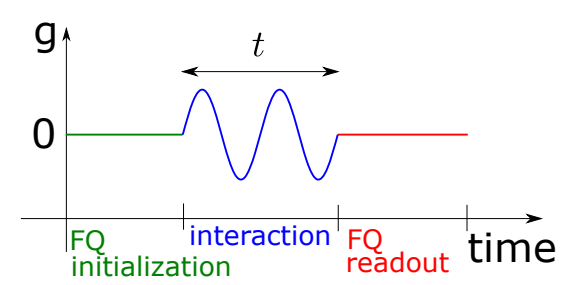


FIG. 2. Schematic of the time dependence of g(t). To induce an interaction between the FQ and the spin ensemble, we modulate the coupling strength to oscillate.

V. ENTANGLEMENT GENERATION BETWEEN THE ELECTRON SPINS VIA REPETITIVE MEASUREMENTS WITH THE FQ

In this section, we show our second main result that the SQL-beating states are generated under the evolution of the spin ensemble's state through a sequence of Ramsey-type measurements involving the FQ. With the ground state at temperature zero as the initial state of the spin ensemble, we obtain a certain Dicke state after infinitely many readout processes in a reasonable parameter regime. We see that the probability of obtaining a generalized cat state as a final state is asymptotically 1 for large N.

A. State after m measurements

In this subsection, we consider what state we get after m measurements are applied to the spin ensemble. Let $\hat{\rho}_{\rm P}(m)$ denote the density matrix of the spin ensemble after the mth measurement by the FQ, where $\hat{\rho}_{\rm P}(0)$ is given by Eq. (23). By performing (m+1)th measurement on $\hat{\rho}_{\rm P}(m)$, one obtains either of the following,

$$\hat{\rho}_{P}(m+1) = \frac{\hat{W}_{+}\hat{\rho}_{P}(m)\hat{W}_{+}^{\dagger}}{\text{Prob}[\Sigma_{2} = +1]},$$
(34)

$$\hat{\rho}_{P}(m+1) = \frac{\hat{W}_{-}\hat{\rho}_{P}(m)\hat{W}_{-}^{\dagger}}{\text{Prob}[\Sigma_{2} = -1]},$$
(35)

depending on the measurement results, where

$$\hat{W}_{+} := \langle +_{y} | e^{-i\frac{g}{2}\hat{S}_{x}\otimes\hat{\Sigma}_{3}t} | + \rangle = \frac{1-i}{\sqrt{2}}\sin\left(\frac{\pi}{4} + \frac{gt\hat{S}_{x}}{2}\right),\tag{36}$$

$$\hat{W}_{-} := \langle -_{y} | e^{-i\frac{g}{2}\hat{S}_{x} \otimes \hat{\Sigma}_{3}t} | + \rangle = \frac{1+i}{\sqrt{2}} \sin\left(\frac{\pi}{4} - \frac{gt\hat{S}_{x}}{2}\right)$$
(37)

are measurement operators. For detailed derivation, see Appendix A. Here, $|\pm_y\rangle$ denotes the eigenvectors of $\hat{\Sigma}_2$ with an eigenvalue of ± 1 . The probability for the corresponding projection is given by

$$\operatorname{Prob}[\Sigma_2 = \pm 1] = \operatorname{Tr}(\hat{W}_{\pm}\hat{\rho}_{\mathrm{P}}(m)\hat{W}_{\pm}^{\dagger}). \tag{38}$$

To elucidate the effect of repetitive measurements, we study the zero-temperature limit $\beta \to \infty$ in this section, and leave the study of the case of finite temperature in the next section. In the zero-temperature limit, the initial state of the spin ensemble is a pure state $|\uparrow\rangle^{\otimes N}$. Hence we analyze $|\phi_m\rangle$, a pure state after m measurements. At each readout process, either \hat{W}_+ or \hat{W}_- is probabilistically applied to the state of the spin ensemble. This means there are 2^m possible trajectories when m measurements are performed by the FQ. Fortunately, since \hat{W}_+ commutes with \hat{W}_- , the number of effective trajectories is reduced, and there are only (m+1) distinct trajectories to consider. Let k denote the number of times \hat{W}_+ is applied to the state during the m measurements. For a given k, the final state can be expressed as

$$|\phi_m\rangle = (\hat{W}_+)^k (\hat{W}_-)^{m-k} |\uparrow\rangle^{\otimes N} / (\text{norm}),$$
 (39)

where

$$(\text{norm}) = \langle \uparrow |^{\otimes N} (\hat{W}_{+}^{\dagger} \hat{W}_{+})^{k} (\hat{W}_{-}^{\dagger} \hat{W}_{-})^{m-k} | \uparrow \rangle^{\otimes N}. \quad (40)$$

Assuming

$$qtN < \pi/2 \tag{41}$$

for simplicity for a while, we can prove that for $m \gg 1$, $(\hat{W}_+)^k(\hat{W}_-)^{m-k}$ attains the eigenvalue with the largest modulus for eigenstates of \hat{S}_x , when the corresponding eigenvalue

 S_x becomes the closest to $(gt)^{-1} \arcsin(2k/m-1)$. Details are provided in the Appendix B.

Importantly, it is known that if an operator \hat{K} is applied infinitely many times to the system, the system converges to the eigenstate of \hat{K} corresponding to the eigenvalue with the largest modulus, provided it is unique [76–78]. Furthermore, in our case, we obtain $(\hat{W}_+)^k(\hat{W}_-)^{m-k}=((\hat{W}_+)^\alpha(\hat{W}_-)^{(1-\alpha)})^m$ for $k=\alpha m$ where $0\leq\alpha\leq1$. It is worth mentioning that $\hat{K}=(\hat{W}_+)^\alpha(\hat{W}_-)^{(1-\alpha)}$ and $(\hat{W}_+)^k(\hat{W}_-)^{m-k}$ take the largest eigenvalue with the same eigenstate. By applying this fact to our case, we obtain

$$|\phi_m\rangle \simeq \left|S_x = (gt)^{-1}\arcsin\left(\frac{2k}{m} - 1\right)\right\rangle,$$
 (42)

for large m, if we assume that $(gt)^{-1}\arcsin\left(\frac{2k}{m}-1\right)$ is integer. Here, we define

$$|S_x = \theta\rangle := |D_N^{(\theta)}\rangle, \tag{43}$$

where $|D_N^{(\theta)}\rangle$ is a Dicke state given by

$$|D_N^{(\theta)}\rangle = \sqrt{\left(\frac{N}{\frac{N+\theta}{2}}\right)^{-1}} \sum_{\sigma \in \mathcal{S}_N} \mathcal{P}_{\sigma} \left(|+\rangle^{\otimes (N+\theta)/2} |-\rangle^{\otimes (N-\theta)/2} \right),$$
(44)

with \mathcal{P}_{σ} denoting the permutation of spins and the summation taken over all different permutations in the permutation group S_N [79–81].

For an illustration, consider the example where k=m/2 for an even number m. An operator $\hat{W}_+\hat{W}_-=\cos(gt\hat{S}_x)/2$ is applied m/2 times. In the region $-\pi/2 < x < \pi/2$, the function $\cos(x)$ attains its maximum value of 1 at x=0. Therefore, we obtain

$$|\phi_m\rangle \to |S_x = 0\rangle$$
 (45)

in the limit of $m \to \infty$.

Note that S_x takes only integer values, while $(gt)^{-1}\arcsin\left(\frac{2k}{m}-1\right)$ is not necessarily an integer. This necessitates refining the formula (42) as follows. In the limit of $m\to\infty$, the final state converges to

$$\lim_{m \to \infty} |\phi_m\rangle = |S_x = L\rangle, \tag{46}$$

where L is the integer closest to $(gt)^{-1} \arcsin{(2k/m-1)}$. If $(gt)^{-1} \arcsin{(2k/m-1)}$ is a half-integer, there are two possible states with eigenvalues whose modulus are the largest. In this case, the final state depends on the initial state's weight about these two states. This idea can be applied also in the next paragraph.

In actual experiments, it is not always possible to satisfy the condition of $gtN < \pi/2$. In a region $gtN \ge \pi/2$, the operator $(\hat{W}_+)^k(\hat{W}_-)^{m-k}$ takes the eigenvalue with the largest modulus when S_x takes either of the following values:

$$\theta_1(n) := \left(\arcsin\left(\frac{2k}{m} - 1\right) + 2n\pi\right)/(gt), \quad (47)$$

$$\theta_2(n') := \left(\pi - \arcsin\left(\frac{2k}{m} - 1\right) + 2n'\pi\right)/(gt). \quad (48)$$

Here, n and n' are integers that satisfy

$$-gtN \le \arcsin(\frac{2k}{m} - 1) + 2n\pi \le gtN, \tag{49}$$

$$-gtN \le \pi - \arcsin(\frac{2k}{m} - 1) + 2n'\pi \le gtN, \qquad (50)$$

where we use $-N \leq S_x \leq N$. As we have discussed in the previous paragraph, the final state should be $|S_x = L\rangle$, where L is the integer closest to the largest (in magnitude) eigenvalue of $(\hat{W}_+)^k(\hat{W}_-)^{m-k}$, among $\theta_1(n)$ and $\theta_2(n')$ with multiple candidates of ns and n's (we assume that such L is unique for simplicity). That implies that the integer L is taken as

$$L = \begin{cases} \theta_1(n) & (\min_{n \in \mathbb{Z}} h_1(n) \le \min_{n' \in \mathbb{Z}} h_2(n')) \\ \theta_2(n') & (\min_{n \in \mathbb{Z}} h_1(n) > \min_{n' \in \mathbb{Z}} h_2(n')) \end{cases}$$
(51)

where

$$h_1(n) := |\theta_1(n) - \text{Round}(\theta_1(n))|, \qquad (52)$$

$$h_2(n') := |\theta_2(n) - \text{Round}(\theta_2(n))|.$$
 (53)

Here, $\operatorname{Round}(x)$ is the integer closest to x.

B. Variance of \hat{S}_z in $\hat{\rho}_P(m)$

Next, we examine whether these post-measurement states are generalized cat states. As we have clarified in the previous subsection, the final state, i.e., $\hat{\rho}_{\rm P}(m)$ with $m \to \infty$, is a pure state when the initial state is a pure state $|\uparrow\rangle^{\otimes N}$. If the variance of an additive observable is of the order of N^2 , such a pure state is a generalized cat state [51, 52].

Calculating the variance of \hat{S}_z for $|S_x = \xi\rangle$, we obtain

$$\langle S_x = \xi | \hat{S}_z^2 | S_x = \xi \rangle - \langle S_x = \xi | \hat{S}_z | S_x = \xi \rangle^2$$

$$= \frac{N^2 - \xi^2}{2} + N. \tag{54}$$

This shows that, as long as there exists a positive N-independent constant δ (< 1) such that $|\xi/N| < 1 - \delta$ is satisfied, $|S_x = \xi\rangle$ is a generalized cat state. In the case $gtN < \pi/2$, the final state $|S_x \simeq (gt)^{-1} \arcsin((2k-m)/m)\rangle$ is a generalized cat state if there exists a positive constant δ' (< 1) such that $|(Ngt)^{-1} \arcsin((2k-m)/m)| < 1 - \delta'$ is satisfied, assuming for simplicity that L in the previous subsection is uniquely determined. Intuitively, this can be explained as follows: generalized cat states are produced by the m measurements when k is far enough from 0 and m so that $(gt)^{-1} \arcsin((2k-m)/m)$ is not as large as N.

C. Probability of trajectories

We investigate the success probability of creating a generalized cat state when the initial state is $|\uparrow\rangle^{\otimes N}$.

Let p(k) denote the probability of obtaining the trajectories in which \hat{W}_+ is applied k times. Since there are $\binom{m}{k}$ trajectories for a given k, the probability p(k) is calculated as (see Appendix C for derivation)

$$p(k) = \binom{m}{k} \langle \uparrow |^{\otimes N} \left(\hat{W}_{+}^{\dagger} \hat{W}_{+} \right)^{k} \left(\hat{W}_{-}^{\dagger} \hat{W}_{-} \right)^{m-k} | \uparrow \rangle^{\otimes N}$$

$$= \binom{m}{k} \frac{1}{2^{N}} \sum_{k=0}^{N} \binom{N}{r}$$
(55)

$$= {m \choose k} \frac{1}{2^N} \sum_{r=0}^{\infty} {n \choose r} \times \left(\frac{1 + \sin(gt(2r-N))}{2}\right)^k \left(\frac{1 - \sin(gt(2r-N))}{2}\right)^{m-k}.$$
(56)

This p(k) exhibits markedly different behaviors for various parameters (Fig. 3). For $gtN < \pi/2$, there are two highest peaks near k = m/2 for odd N, whereas there is a single highest peak at k = m/2 for even N. Additionally, the probabilities p(0) and p(m) are small.

Notably, we can prove that success probability of generating a generalized cat state is sufficiently large. In particular, we can show that the probability approaches 1 as

$$\lim_{N \to \infty} \lim_{m \to \infty} \sum_{k}' p(k) = 1 \quad \text{when } gtN < \pi/2, \qquad (57)$$

where \sum_k' denotes the sum taken over k such that the corresponding stationary states are the generalized cat states. In fact, in the limit $m \to \infty$, p(k) can be regarded as a sum of the sharp normal-distribution peaks (as in Fig. 3(left)). Then, taking $N \to \infty$ leads to the concentration of the peaks towards $k \simeq m/2$, resulting in $\sum_k' p(k) \to 1$. For the detailed proof, see Appendix D. This is intuitively because we obtain a generalized cat state unless k is close to k0 or k1 when k2, which is unlikely as already speculated from Fig. 3(left).

For $gtN \geq \pi/2$, p(k) exhibits a different behavior (see Fig. 3(right)). We observe that p(0) and p(m) have relatively large values. However, we still obtain generalized cat states with a reasonable success probability, as we numerically find in the next section.

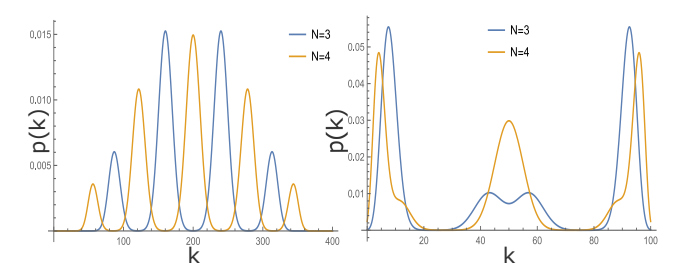


FIG. 3. Plot of the probability p(k) of obtaining the trajectories in which \hat{W}_+ is applied k times, as described in Eq. (56), against k. On the left, the parameters are gt=0.2, m=400, N=3 (blue) and N=4 (yellow), satisfying $gtN<\pi/2$. In this case, p(k) is approximately given by a sum of the sharp normal-distribution-like peaks, whose heights become larger when they are closer to k=m/2. On the right, the parameters are gt=1.0, m=100, N=3 (blue) and N=4 (yellow), satisfying $gtN \ge \pi/2$.

D. Required number of the measurements

As explained in Sec. V A, infinite number of measurements convert the initial state to $|S_x = L\rangle$. In this subsection, we discuss how many measurements are required to approximately obtain this stationary state, assuming the case $gtN < \pi/2$.

For this purpose, we evaluate the spectral gap characterizing the dynamics. More precisely, we consider the spectrum $\{\lambda_a\}$ $(\lambda_1 \leq \lambda_2 \leq \cdots)$ of an operator

$$-\frac{1}{2m}\ln\left(\hat{W}_{+}^{k}\hat{W}_{-}^{m-k}\right)\left(\hat{W}_{+}^{k}\hat{W}_{-}^{m-k}\right)^{\dagger} = -\frac{1}{2}\ln\hat{K}\hat{K}^{\dagger} \tag{58}$$

with $\hat{K}=\hat{K}^\dagger=(\hat{W}_+)^\alpha(\hat{W}_-)^{1-\alpha}$ and $\alpha=k/m$, which is called the Lyapunov spectrum of a trajectory under measurement [82, 83]. The inverse of the gap of the Lyapunov spectrum, $\lambda_2-\lambda_1$, is known to provide the timescale for relaxation to the final state. This is because the ratio of weights between the longest-lived decaying mode and the final state is evaluated by $e^{-\lambda_2 m}/e^{-\lambda_1 m}$, which becomes $\sim e^{-1}$ when $m \simeq m_{\rm relax} := (\lambda_2 - \lambda_1)^{-1}$.

Since \hat{W}_{\pm} are diagonal in the \hat{S}_x basis, the above operator is simply given by

$$-\ln f(gt\hat{S}_x),\tag{59}$$

where $f(x):=\sin^{\alpha}\left(\frac{\pi}{4}+\frac{x}{2}\right)\sin^{1-\alpha}\left(\frac{\pi}{4}-\frac{x}{2}\right)$ (see Appendix B). In App. B, we show that f(x) takes a maximum value when

$$x_* = \arcsin(2\alpha - 1), \tag{60}$$

which leads to Eq. (42) and $\lambda_1 = -\ln f(x_*)$ if x_*/gt is an integer. If x_*/gt is not an integer, we instead have

$$\lambda_1 = -\ln f(gtL) \tag{61}$$

with $L = \text{Round}(x_*/gt)$.

Next, since f(x) is a concave function taking the maximum at $x=x_*$ (App. B) and S_x takes integer values, we can evaluate λ_2 as

$$\lambda_2 = -\ln f(gtL + gt) \tag{62}$$

or

$$\lambda_2 = -\ln f(gtL - gt). \tag{63}$$

Let us first assume that x_*/gt is an integer, i.e., $gtL = x_*$. Then, assuming $gt \ll 1$, we can evaluate the gap at the leading order of $(gt)^2$ from the form of f(x), finding

$$\lambda_2 - \lambda_1 \simeq \frac{(gt)^2}{4}. (64)$$

This leads to the relaxation timescale

$$m_{\rm relax} \simeq \frac{4}{(at)^2}.$$
 (65)

Interestingly, this does not explicitly depend on α .

When x_*/gt is not an integer, the gap becomes smaller than $(gt)^2/4$, but remains the order of $(gt)^2$, unless it accidentally vanishes. Therefore, we conclude that the relaxation time for most measurement outcomes becomes the order of $m_{\rm relax} \sim (gt)^{-2}$.

VI. NUMERICAL SIMULATIONS

In this section, we study the case of finite temperature using numerical simulations. The initial state of the spin ensemble is a mixed state, i.e., a thermal equilibrium state subjected to a magnetic field h along the z axis. The quantity that we mainly focus on is what we call "catness," which is defined as $\frac{1}{2}\|[\hat{S}_z,[\hat{S}_z,\hat{\rho}_P(m)]]\|_1$. If it is $\Theta(N^q)$ with q>1.5, the state is a SQL-beating cat-like state, as discussed in Sec. III. To visualize the emergence of generalized cat states we numerically compute the value of $\frac{1}{2}\|[\hat{S}_z,[\hat{S}_z,\hat{\rho}_P(m)]]\|_1$ for each m up to m=1000. In the following, we take $1/\beta=0.1$ and h=0.5. The interaction strength between the FQ and the spin ensemble is set to be gt=0.222. This is the case where $gtN>\pi/2$, which we did not analytically discuss above. Remarkably, we can see the emergence of SQL-beating cat-like state even in this regime.

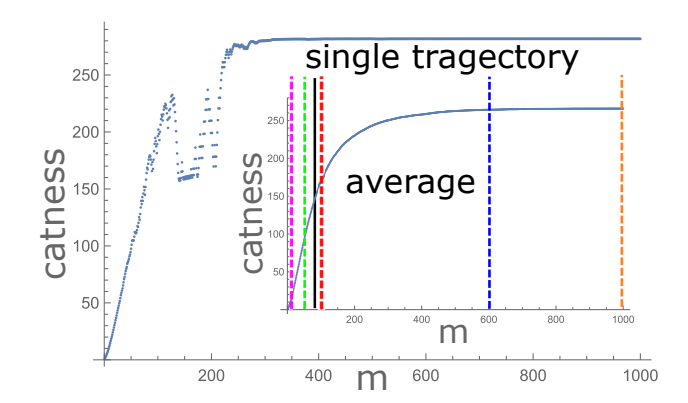


FIG. 4. Visualization of the creation of generalized cat states through repetitive measurements with N=15 qubits. The horizontal axis represents the number of measurements with the FQ, while the vertical axis denotes the value of catness $(\frac{1}{2}\|[\hat{S}_z,[\hat{S}_z,\hat{\rho}_{\rm P}(m)]]\|_1)$. Due to the probabilistic nature of each measurement, the values of catness exhibit temporal fluctuations within a single trajectory. The inset illustrates the results averaged over 3000 runs. In the inset, black vertical line shows $m=82\simeq m_{\rm relax}$. Purple, green, red, blue and orange lines in inset indicate m=10,50,100,600,1000, respectively. This average reveals a clear, gradual increase in catness. The initial state is $\exp(-\beta h \hat{S}_z)/{\rm Tr} \exp(-\beta h \hat{S}_z)$ with $1/\beta=0.1$, h=0.5, and a coupling strength multiplied by the interaction time given by gt=0.222.

A. Trajectories for a fixed N

Let us examine a single trajectory for a fixed $N \ (= 15)$, depicted in Fig. 4. In each trajectory, the measurement outcome at each m is probabilistically determined, and the measurement-backaction from each result influences the catness value. Due to the stochastic nature of these measurements, a single trajectory exhibits temporal fluctuations, albeit with an overall tendency for the catness to increase. By averaging over 3000 trajectories, we observe that the catness undergoes rapid changes initially but becomes almost constant around $m \sim 600$, as shown in the inset of Fig. 4. Note that at $m_{\rm relax} \simeq 4/(gt)^2 \simeq 82$, the value of catness is 147, which is near the half of the stationary catness, even though we here consider the case $gtN > \pi/2$.

B. Scaling behavior of the catness

To determine whether we have successfully created a generalized cat state, it is essential to examine the scaling behavior of the catness with respect to N at each m. For $N=3,\,5,\,7,\,15,\,31,\,63,\,127$, we average 3000 random trajectories and plot the catness value in Fig. 5. A linear fit is performed to determine the slope of the line, corresponding to the index q. As depicted, the slope increases with m, but does not show a significant change after $m\sim 600$.

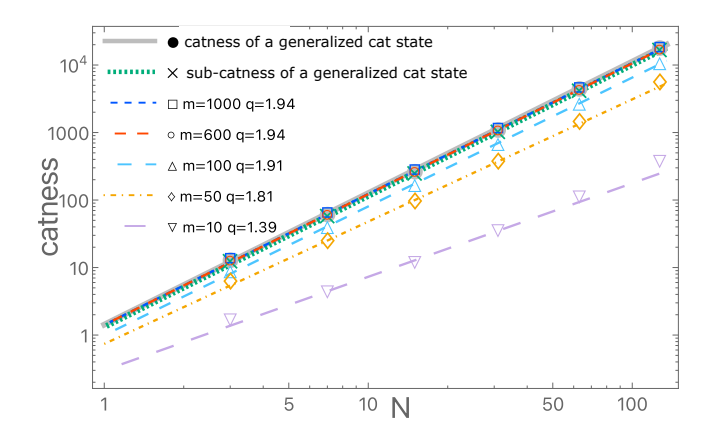


FIG. 5. Log-log plot of the catness value against N for different m values, along with two reference plots. From the bottom to the top, the m values are m = 10 (purple), 50 (orange), 100 (cvan), 600 (red), 1000 (blue), respectively. The initial state is given by $\exp(-\beta h \hat{S}_z)/\operatorname{Tr} \exp(-\beta h \hat{S}_z)$ with $1/\beta = 0.1$, h = 0.5, and a coupling strength of gt = 0.222. The thick gray line represents the reference obtained from Eq. (66), which is a catness of a generalized cat state. Green dotted line represents the reference obtained from Eq. (67), which we call a sub-catness of a generalized cat state. Error bars were omitted as they were smaller than the widths of the dots.

With a linear fit using the data for N3, 5, 7, 15, 31, 63, 127, we obtain up to q = 1.94 at m = 1000, which is sufficiently close to the generalized cat state with q = 2. Since q > 1.5 is achieved already for m = 50, we can create SQL-beating cat-like states by this timescale.

Note that, for a reference, Fig. 5 also shows two additional curves: they are concerning a generalized cat state obtained by a single projective measurement $\hat{\mathcal{P}}(M)$ [50] (see Sec. II B), where the initial state is the zero-temperature pure state, $\hat{\rho}_{\mathrm{pure}} = |\uparrow\rangle^{\otimes N} \langle\uparrow|^{\otimes N}$. One curve describes the catness of the post-measurement state averaged over outcomes $M = -N, -N + 2, \cdots, N$ for the projection measurement,

$$\sum_{M=-N,N-2,...,N} \frac{1}{2^N} \binom{N}{\frac{N+M}{2}} \| [\hat{S}_z, [\hat{S}_z, \hat{\mathcal{P}}(M) \hat{\rho}_{\text{pure}} \hat{\mathcal{P}}(M)] \|_1$$

where $\binom{N}{(N+M)/2}/2^N$ is the corresponding probability. Since this is at zero temperature, this curve shows the highest value of catness among any temperature. The second curve describes what we call the sub-catness, which provides the analytically tractable lower bound of Eq. (66). Motivated by the intuitive measurement protocol explained in Sec. II B, the subcatness is defined as the zero-temperature limit $(\beta \to \infty)$ of Eq. (5) averaged over all measurement outcomes, i.e.,

$$\sum_{M=-N,N-2,...,N} \frac{1}{2^N} {N \choose \frac{N+M}{2}} \operatorname{Tr}(\hat{\mathcal{P}}(M)[\hat{S}_z, [\hat{S}_z, \hat{\rho}_{PM}]])$$

$$= \sum_{M=-N,N-2,...,N} \frac{1}{2^N} {N \choose \frac{N+M}{2}} (N^2 - M^2 + 2N). (67)$$

As can be seen in Fig. 5, the fitted line of the state after 600 measurements is indistinguishable from the plot for the generalized cat state generated from the catness and subcatness curves for the single projective measurement under zero temperature $\hat{\rho}_{\text{pure}}$. This implies that the repetitive measurements we consider in this paper can indeed replace with the single projective-measurement scheme in Ref [50], which required considerably high-resolution measurement. It is also remarkable that our scheme is comparable to the single projectivemeasurement scheme under zero temperature, even though we consider nonzero temperature.

Finally, we note that within this numerical simulation, we cannot achieve $\Theta(N^2)$ scaling of catness from the fitting. The possible reasons for this are as follows. Firstly, we considered the region $gtN > \pi/2$ in the numerical simulation, while we proved (57) assuming $gtN < \pi/2$. Secondly, unless N is infinitely large, there will be a finite contribution from both $\Theta(N^2)$ and $\Theta(N)$ terms. When we substitute N = 3, 5, 7, 15, 31, 63, 127 in Eq. (67) and Eq. (66) and perform the linear fitting in the same manner, we obtain q = 1.95, which is less than 2, even when accounting for fitting error. Consequently, it is challenging to obtain catness with the scaling $\Theta(N^2)$ from numerical simulations up to N=127. Nonetheless, our results are still significant as they demonstrate the potential of utilizing this highly entangled state with q > 1.5 for quantum sensing, as we discussed above.

C. Sensitivity of the generated states

Let us calculate the sensitivity of the states with q > 1.5that are generated through the repetitive measurements. We consider the case where N=127. Substituting the value of catness for Eq. (20), we show $\delta\omega$ of the following states in Table I: state at m = 50 with q = 1.81, state at m = 100 with q = 1.91, state at m = 600 with q = 1.94, and generalized cat $\sum_{M=-N,N-2,\dots,N} \frac{1}{2^N} \binom{N}{\frac{N+M}{2}} \|[\hat{S}_z,[\hat{S}_z,\hat{\mathcal{P}}(M)\hat{\rho}_{\mathrm{pure}}\hat{\mathcal{P}}(M)]]\|_1 \\ \text{We also calculate the sensitivity of a separable state using a known formula } \delta\omega = \frac{1}{2\sqrt{N}\sqrt{Tt_{\mathrm{int}}}}.$

TABLE I. Comparison of sensitivity of states with various q. Uncertainty $\delta\omega$ for states with q=1,1.81,1.91,1.94,2 are calculated. We can see a clear advantage of q > 1.5.

| \overline{m} | q | $\delta \omega$ |
|----------------|---------------------------|---|
| - | 1 (separable state) | $4.4 \times 10^{-2} / \sqrt{Tt_{\rm int}}$ |
| 50 | 1.81 | $\leq 2.4 \times 10^{-2} / \sqrt{Tt_{\rm int}}$ |
| 100 | 1.91 | $\leq 1.2 \times 10^{-2} / \sqrt{Tt_{\rm int}}$ |
| 600 | 1.94 | $\leq 7.4 \times 10^{-3} / \sqrt{Tt_{\rm int}}$ |
| | 2 (generalized cat state) | $\leq 7.0 \times 10^{-3} / \sqrt{Tt_{\rm int}}$ |

From this table, it is clear that states with q > 1.5, produced via moderate number of measurements, are indeed advantageous in quantum sensing than a separable state.

VII. CONCLUSION

We studied the relation between $\delta\omega$ and q and derived an inequality $\delta\omega \leq O(N^{1-q})$. Any state with q>1.5 is advantageous in quantum metrology, hence we call states with q > 1.5 SQL-beating cat-like states. Then we proposed a method to create SQL-beating cat-like states through repetitive measurements. A thermal equilibrium state of the spin ensemble is coupled with an ancillary qubit, and we repeatedly measure the ancillary qubits. This sequential measurement of the ancillary qubit provides information about the total magnetization of the spins, leading the spin ensemble to gradually approach the SQL-beating cat-like states. Notably, no dynamical control over the spin ensembles is required during the creation of these states. Analytically, we demonstrate that the final state is likely to become a SQL-beating cat-like state when the initial state is pure, i.e., at zero temperature. For a mixed state at finite temperature as the initial state, we numerically show that SQL-beating cat-like states can be created via repetitive measurements. Our proposal is feasible using a superconducting flux qubit and an electron spin ensemble. These results pave the way for the realization of entanglement-enhanced metrology.

ACKNOWLEDGMENTS

M.T. was supported by the Japan Society for the Promotion of Science through a JSPS fellowship (JSPS KAK-ENHI Grant No. 22KJ3175). This work was supported by JST Moonshot (Grant Number JPMJMS226C). Y Matsuzaki was supported by JSPS KAKENHI (Grant Number 23H04390). This work was supported by CREST (JPMJCR2315, 20H05661), JST. R.H. was supported by JST ERATO Grant Number JPMJER2302, Japan, and JSPS KAK-ENHI Grant No. JP24K16982. A.S. is supported by Japan Society for the Promotion of Science KAKENHI Grant No. 23K22413.

DATA AVAILABILITY

The data are available from the authors upon reasonable request.

Appendix A: Derivation of the state after (m+1)th measurement

Let us investigate $\hat{\rho}_{\mathrm{P}}(m+1)$, the state after (m+1)th measurement, from $\hat{\rho}_{\mathrm{P}}(m)$. Measurement protocol is as follows. First, we initialize the FQ so that the initial state is $\hat{\rho}_{\mathrm{P}}(m) \otimes |+\rangle \langle +|$. Then, we let the total state evolve with the Hamiltonian $\hat{H}_{\mathrm{R}} = \frac{g}{2}\hat{S}_x \otimes \hat{\Sigma}_3$. Lastly, we read out the FQ on $\hat{\Sigma}_2$ basis $(\hat{\Sigma}_2 |\pm_y\rangle = |\pm_y\rangle$). If we obtain +1 as an outcome of the measurement, then $\hat{\rho}_{\mathrm{P}}(m+1) = \hat{\rho}_{\mathrm{P}}(m+1)_+$, which

is written as

$$\hat{\rho}_{P}(m+1)_{+}$$

$$=\frac{\langle +_{y}|e^{-i\frac{g}{2}\hat{S}_{x}\otimes\hat{\Sigma}_{3}t}\hat{\rho}_{P}(m)\otimes|+\rangle\langle +|e^{i\frac{g}{2}\hat{S}_{x}\otimes\hat{\Sigma}_{3}t}|+_{y}\rangle}{\text{Prob}[\Sigma_{2}=+1]}$$
(A1)

$$=\frac{\hat{W}_{+}\hat{\rho}_{\mathrm{P}}(m)\hat{W}_{+}^{\dagger}}{\mathrm{Prob}[\Sigma_{2}=+1]},\tag{A2}$$

where

$$\hat{W}_{+} = \langle +_{y} | e^{-i\frac{g}{2}\hat{S}_{x} \otimes \hat{\Sigma}_{3}t} | + \rangle \tag{A3}$$

$$=\frac{e^{-i\frac{g}{2}t\hat{S}_{x}}-ie^{i\frac{g}{2}t\hat{S}_{x}}}{2}$$
 (A4)

$$=\frac{1-i}{\sqrt{2}}\sin\left(\frac{\pi}{4}+\frac{gt}{2}\hat{S}_x\right) \tag{A5}$$

and

$$Prob[\Sigma_{2} = +1]$$

$$= Tr\left(\langle +_{y}|e^{-i\frac{g}{2}\hat{S}_{x}\otimes\hat{\Sigma}_{3}t}\hat{\rho}_{P}(m)\otimes |+\rangle\langle +|e^{i\frac{g}{2}\hat{S}_{x}\otimes\hat{\Sigma}_{3}t}|+_{y}\rangle\right).$$
(A6)

Similarly, if we obtain -1 as an outcome of the measurement, then $\hat{\rho}_{\rm P}(m+1) = \hat{\rho}_{\rm P}(m+1)_-$, which is written as

$$\hat{\rho}_{P}(m+1)_{-}$$

$$=\frac{\langle -_{y}|e^{-i\frac{g}{2}\hat{S}_{x}\otimes\hat{\Sigma}_{3}t}\hat{\rho}_{P}(m)\otimes|+\rangle\langle +|e^{i\frac{g}{2}\hat{S}_{x}\otimes\hat{\Sigma}_{3}t}|-_{y}\rangle}{\text{Prob}[\Sigma_{2}=-1]}$$
(A7)

$$=\frac{\hat{W}_{-}\hat{\rho}_{\mathrm{P}}(m)\hat{W}_{-}^{\dagger}}{\mathrm{Prob}[\Sigma_{2}=-1]},\tag{A8}$$

where

$$\hat{W}_{-} = \langle -_{y} | e^{-i\frac{g}{2}\hat{S}_{x} \otimes \hat{\Sigma}_{3} t} | + \rangle \tag{A9}$$

$$= \frac{e^{-i\frac{g}{2}t\hat{S}_x} + ie^{i\frac{g}{2}t\hat{S}_x}}{2}$$
 (A10)

$$= \frac{1+i}{\sqrt{2}} \sin\left(\frac{\pi}{4} - \frac{gt}{2}\hat{S}_x\right) \tag{A11}$$

and

$$Prob[\Sigma_{2} = -1]$$

$$= Tr\left(\langle -_{y}|e^{-i\frac{g}{2}\hat{S}_{x}\otimes\hat{\Sigma}_{3}t}\hat{\rho}_{P}(m)\otimes|+\rangle\langle +|e^{i\frac{g}{2}\hat{S}_{x}\otimes\hat{\Sigma}_{3}t}|-_{y}\rangle\right).$$
(A12)

Appendix B: Derivation of $|\phi_m\rangle$

Here, let us discuss the state we get after applying $\hat{W}_{+}^{k}\hat{W}_{-}^{m-k}$, where $0 \leq k \leq m$ is the number of \hat{W}_{+} applied in m measurements. There is a theorem that when an operator \hat{K} is applied for infinite times, the state converges

to the eigenstate of \hat{K} with the eigenvalue whose modulus is the largest, provided that it is nondegenerate. Furthermore, in our case, for $k=\alpha m$ where $0<\alpha<1$, we obtain $(\hat{W}_+)^k(\hat{W}_-)^{m-k}=((\hat{W}_+)^\alpha(\hat{W}_-)^{(1-\alpha)})^m$. By taking $\hat{K}:=(\hat{W}_+)^\alpha(\hat{W}_-)^{(1-\alpha)}$, we can adopt this theorem.

We want to find the largest (in magnitude) eigenvalue of

 \hat{K}

$$= \left(\frac{1-i}{\sqrt{2}}\sin(\frac{\pi}{4} + \frac{gt}{2}\hat{S}_x)\right)^{\alpha} \left(\frac{1+i}{\sqrt{2}}\sin(\frac{\pi}{4} - \frac{gt}{2}\hat{S}_x)\right)^{1-\alpha}$$
(B1)

for each α . When \hat{K} is applied to some initial state $|\psi_0\rangle=\sum_l c_l\,|S_x=l\rangle$, then

$$\hat{K} |\psi_0\rangle = \left(\frac{1-i}{\sqrt{2}}\right)^{\alpha} \left(\frac{1+i}{\sqrt{2}}\right)^{1-\alpha} \times \sin^{\alpha} \left(\frac{\pi}{4} + \frac{gt}{2}\hat{S}_x\right) \sin^{1-\alpha} \left(\frac{\pi}{4} - \frac{gt}{2}\hat{S}_x\right) \sum_{l} c_l |S_x = l\rangle$$
(B2)

$$= \left(\frac{1-i}{\sqrt{2}}\right)^{\alpha} \left(\frac{1+i}{\sqrt{2}}\right)^{1-\alpha} \times \sum_{l} c_{l} \sin^{\alpha} \left(\frac{\pi}{4} + \frac{gt}{2}l\right) \sin^{1-\alpha} \left(\frac{\pi}{4} - \frac{gt}{2}l\right) |S_{x} = l\rangle.$$
(B3)

Let us define f(x) as follows.

$$f(x) := \sin^{\alpha}\left(\frac{\pi}{4} + \frac{x}{2}\right)\sin^{1-\alpha}\left(\frac{\pi}{4} - \frac{x}{2}\right)$$
 (B4)

Finding the extremum of f(x) corresponds to finding the largest eigenvalue of \hat{K} because \hat{W}_{\pm} are diagonal in the \hat{S}_x basis.

To find the extremum, we take derivative

$$f'(x) = \frac{2\alpha - 1 - \sin x}{4\sin^{1-\alpha}\left(\frac{\pi}{4} + \frac{x}{2}\right)\sin^{\alpha}\left(\frac{\pi}{4} - \frac{x}{2}\right)}.$$
 (B5)

We can see that f(x) takes the extremum at x that satisfies g(x) = 0, where

$$g(x) := 2\alpha - 1 - \sin x. \tag{B6}$$

It is obvious that g(x) takes zero at

$$\sin x = 2\alpha - 1. \tag{B7}$$

For simplicity, let us first consider the region

$$-\frac{\pi}{2} < x < \frac{\pi}{2}.\tag{B8}$$

Since $0 < \alpha < 1$, f(x) takes the maximum at $x = \arcsin(2\alpha - 1)$, which is greater than 0 and smaller than $\pi/2$. When $\alpha = 1$ (-1), f(x) takes the maximum (minimum) 1

TABLE II. Derivative test chart of f(x). It increases until $x = \arcsin(2\alpha - 1)$ and then decreases.

| \overline{x} | $-\pi/2$ | $\arcsin(2\alpha - 1)$ | $\pi/2$ |
|----------------|----------|------------------------|------------|
| f'(x) | + | 0 | _ |
| f(x) | 7 | | \searrow |

(-1) at $x=\pi/2$ $(-\pi/2).$ These can be illustrated as in Table II.

Therefore, under the assumption $-\pi/2 < x < \pi/2$, the function f(x) takes the maximum at $x = \arcsin(2\alpha - 1)$, leading to the conclusion that after applying \hat{K} for $m \gg 1$ times, the final state $|\phi_m\rangle$ approaches to (42).

Let us also consider the case of $x \ge \pi/2$ or $x \le -\pi/2$. In general, g(x) takes zero at

$$x = \arcsin(2\alpha - 1) + 2n\pi, \tag{B9}$$

$$x = \pi - \arcsin(2\alpha - 1) + 2n\pi, \tag{B10}$$

where $n \in \mathbb{Z}$. Actually, we can prove that

$$|f(x)| = (1 - \alpha)^{\frac{1 - \alpha}{2}} (\alpha)^{\frac{\alpha}{2}}$$
 (B11)

$$=\sqrt{(1-\alpha)^{1-\alpha}\alpha^{\alpha}}\tag{B12}$$

for any x that satisfies g(x)=0, i.e., $\sin x=2k/m-1$. With the extremums with the equal value of |f(x)|, it implies that there are multiple candidates of the final state. In such a case, we should consider the weight of the eigenstates that are candidates of the final state, in the initial state. That is, the final state should be the superposition of the candidates whose weight is determined by the initial state.

Appendix C: Derivation of p(k)

Here, we explain the derivation of p(k), the probability of obtaining the trajectory with \hat{W}_+ applied k times.

$$\left(\hat{W}_{+}^{\dagger}\hat{W}_{+}\right)^{k} \left(\hat{W}_{-}^{\dagger}\hat{W}_{-}\right)^{m-k} \\
= \left(\sin^{2}(\frac{\pi}{4} + \frac{gt}{2}\hat{S}_{x})\right)^{k} \left(\sin^{2}(\frac{\pi}{4} - \frac{gt}{2}\hat{S}_{x})\right)^{m-k} \\
= \left(\frac{1 + \sin(gt\hat{S}_{x})}{2}\right)^{k} \left(\frac{1 - \sin(gt\hat{S}_{x})}{2}\right)^{m-k} .$$
(C1)

We use $|S_x = 2r - N\rangle$ (where r = 0, 1, ..., N is the number of up spins) in (44) as

$$|S_{x} = 2r - N\rangle = |D_{N}^{(\theta)}\rangle$$

$$= \sqrt{\left(\frac{N}{N+\theta}\right)^{-1}} \sum_{\sigma \in S_{N}} \mathcal{P}_{\sigma} \left(|+\rangle^{\otimes (N+\theta)/2} |-\rangle^{\otimes (N-\theta)/2}\right)$$
(C3)

with $\theta = 2r - N$. Importantly,

$$|\uparrow\rangle^{\otimes N} = \left(\frac{|+\rangle + |-\rangle}{\sqrt{2}}\right)^{\otimes N}$$

$$= \frac{1}{\sqrt{2^N}} \sum_{r=0}^{N} |S_x = 2r - N\rangle \sqrt{\binom{N}{r}}. \tag{C4}$$

Hence we obtain

$$p(k) = \binom{m}{k} \langle \uparrow |^{\otimes N} \left(\hat{W}_{+}^{\dagger} \hat{W}_{+} \right)^{k} \left(\hat{W}_{-}^{\dagger} \hat{W}_{-} \right)^{m-k} | \uparrow \rangle^{\otimes N}$$

$$= \binom{m}{k} \frac{1}{2^{N}} \sum_{r=0}^{N} \langle S_{x} = 2r - N | \sqrt{\binom{N}{r}}$$

$$\times \left(\frac{1 + \sin(gt \hat{S}_{x})}{2} \right)^{k} \left(\frac{1 - \sin(gt \hat{S}_{x})}{2} \right)^{m-k}$$

$$\times \sum_{r'=0}^{N} |S_{x} = 2r' - N \rangle \sqrt{\binom{N}{r'}}$$

$$= \binom{m}{k} \frac{1}{2^{N}} \sum_{r=0}^{N} \binom{N}{r}$$

$$\times \left(\frac{1 + \sin(gt(2r - N))}{2} \right)^{k} \left(\frac{1 - \sin(gt(2r - N))}{2} \right)^{m-k} .$$
(C5)

Appendix D: Probability of obtaining a generalized cat state

We consider the case where m is even. Here discuss the probablity of obtaining a generalized cat state after m measurements with $|\uparrow\rangle^{\otimes N}$ as an initial state. We take the sum of p(k) over k's that allows the emergence of generalized cat states, and prove that it converges to 1 in the limit $N\to\infty$ (note that we take $N\to\infty$ after $m\to\infty$). Probability p(k) can be regarded as a sum of binomial distributions with weight $\binom{N}{r}/2^N$,

$$p(k) = \frac{1}{2^N} \sum_{r=0}^{N} \binom{N}{r} B(gt, r, k),$$
 (D1)

$$B(gt,r) := {m \choose k} s(gt,r)^k (1 - s(gt,r))^{m-k},$$
 (D2)

$$s(gt, r) := \frac{1 + \sin(gt(2r - N))}{2}.$$
 (D3)

If we assume $gtN < \pi/2$, we find s(gt,r) > 0 and 1 - s(gt,r) > 0. Since we are considering large m, the binomial distribution B(gt,r) can be approximated as the normal

distribution, i.e.,

$$B(gt, r, k) \simeq \frac{1}{\sqrt{2\pi m s(gt, r)(1 - s(gt, r))}}$$

$$\times \exp\left(-\frac{(k - m s(gt, r))^2}{2m s(gt, r)(1 - s(gt, r))}\right). \tag{D4}$$

$$\therefore p(k) \simeq \frac{1}{2^N} \sum_{r=0}^N \binom{N}{r} \frac{1}{\sqrt{2\pi m s(gt, r)(1 - s(gt, r))}}$$

$$\times \exp\left(-\frac{(k - m s(gt, r))^2}{2m s(gt, r)(1 - s(gt, r))}\right) \tag{D5}$$

Note that s(gt,r) is a monotonically increasing function of r. Consider the sum of p(k) from $k=m\alpha_1$ to $k=m\alpha_2$. When $m\gg 1$, we can replace the sum with integral, i.e.,

$$\begin{split} &\sum_{k=m\alpha_1}^{m\alpha_2} p(k) \\ &= \sum_{k=m\alpha_1}^{m\alpha_2} \frac{1}{2^N} \sum_{r=0}^N \binom{N}{r} B(gt,r,k) \\ &\simeq \frac{1}{2^N} \sum_{r=0}^N \binom{N}{r} \sqrt{\frac{m}{2\pi s(gt,r)(1-s(gt,r))}} \\ &\times \int_{\alpha_1}^{\alpha_2} d\alpha \exp\left(-\frac{(\alpha-s(gt,r))^2}{2s(gt,r)(1-s(gt,r))}m\right) \\ &\to \frac{1}{2^N} \sum_{r=0}^N \binom{N}{r} \int_{\alpha_1}^{\alpha_2} d\alpha \delta(\alpha-s(gt,r)) \quad (m\to\infty) \end{split} \tag{D8}$$

Here, we substituted $\gamma = \sqrt{\frac{s(gt,r)(1-s(gt,r))}{m}}$ into the following known formula:

$$\lim_{\gamma \to 0} \frac{\exp\left(-\frac{x^2}{2\gamma^2}\right)}{\sqrt{2\pi}\gamma} = \delta(x) \tag{D9}$$

Let us take $\alpha_1 = s(gt, r_1)$ and $\alpha_2 = s(gt, r_2)$. Then the integral is further simplified as follows:

$$\sum_{k=ms(gt,r_1)}^{ms(gt,r_2)} p(k) \simeq \frac{1}{2^N} \sum_{r=r_1}^{r_2} \binom{N}{r}.$$
 (D10)

Now, to evaluate the lower bound of the probability of the emergence of the generalized cat states, we can take $r_1 = Nx_1$ and $r_2 = Nx_2$ with $0 < x_1 < 1/2 < x_2 < 1$ in the above equation. To see that this choice is appropriate, we substitute $k = ms(gt, \tilde{r})$ to Eq. (42), finding

$$|\phi_m\rangle = |S_x = 2\tilde{r} - N\rangle$$
. (D11)

According to Eq. (54), this means that the final state $|\phi_m\rangle$ is indeed a generalized cat state for any $\tilde{r}=Nx$ with 0< x<1.

Then, we finally have

$$\sum_{k=ms(gt,r_1)}^{ms(gt,r_2)} p(k)$$
(D12)

$$= \frac{1}{2^N} \sum_{r=N_T}^{N_{X_2}} \binom{N}{r}$$
 (D13)

$$\simeq \sum_{r=Nx_1}^{Nx_2} \sqrt{\frac{2}{\pi N}} \exp\left(-\frac{2(r-N/2)^2}{N}\right) \tag{D14}$$

$$\to \int_{x_1}^{x_2} dx \delta(x - 1/2) \quad (N \to \infty). \tag{D15}$$

Here, we approximated the binomial distribution in the same manner as we have done with B(gt,r,k), assuming $N\gg 1$. We can immediately see that this approaches to 1 in the limit $N\to\infty$. Therefore, the probability of obtaining a generalized cat state after infinitely many measurements is 1 with $N\to\infty$.

- [1] V. Giovannetti, S. Lloyd, and L. Maccone, Quantum-enhanced measurements: beating the standard quantum limit, Science **306**, 1330 (2004).
- [2] V. Giovannetti, S. Lloyd, and L. Maccone, Advances in quantum metrology, Nature photonics **5**, 222 (2011).
- [3] M. A. Taylor and W. P. Bowen, Quantum metrology and its application in biology, Physics Reports 615, 1 (2016).
- [4] C. L. Degen, F. Reinhard, and P. Cappellaro, Quantum sensing, Reviews of modern physics 89, 035002 (2017).
- [5] D. J. Wineland, J. J. Bollinger, W. M. Itano, F. Moore, and D. J. Heinzen, Spin squeezing and reduced quantum noise in spectroscopy, Phys. Rev. A 46, R6797 (1992).
- [6] D. J. Wineland, J. J. Bollinger, W. M. Itano, and D. J. Heinzen, Squeezed atomic states and projection noise in spectroscopy, Phys. Rev. A 50, 67 (1994).
- [7] G. Tóth and I. Apellaniz, Quantum metrology from a quantum information science perspective, Journal of Physics A: Mathematical and Theoretical 47, 424006 (2014).
- [8] M. G. Paris, Quantum estimation for quantum technology, International Journal of Quantum Information 7, 125 (2009).
- [9] A. W. Chin, S. F. Huelga, and M. B. Plenio, Quantum metrology in non-markovian environments, Phys. Rev. Lett. 109, 233601 (2012).
- [10] R. Chaves, J. B. Brask, M. Markiewicz, J. Kolodyńfiski, and A. Acín, Noisy metrology beyond the standard quantum limit, Phys. Rev. Lett. 111, 120401 (2013).
- [11] J. A. Jones, S. D. Karlen, J. Fitzsimons, A. Ardavan, S. C. Benjamin, G. A. D. Briggs, and J. J. Morton, Magnetic field sensing beyond the standard quantum limit using 10-spin noon states, science 324, 1166 (2009).
- [12] S. F. Huelga, C. Macchiavello, T. Pellizzari, A. K. Ekert, M. B. Plenio, and J. I. Cirac, Improvement of frequency standards with quantum entanglement, Phys. Rev. Lett. 79, 3865 (1997).
- [13] A. Kuzmich, N. Bigelow, and L. Mandel, Atomic quantum nondemolition measurements and squeezing, Europhysics Letters 42, 481 (1998).
- [14] M. Fleischhauer, A. Matsko, and M. Scully, Quantum limit of optical magnetometry in the presence of ac stark shifts, Phys. Rev. A 62, 013808 (2000).
- [15] J. Geremia, J. K. Stockton, A. C. Doherty, and H. Mabuchi, Quantum kalman filtering and the heisenberg limit in atomic magnetometry, Phys. Rev. Lett. 91, 250801 (2003).
- [16] D. Leibfried, M. D. Barrett, T. Schaetz, J. Britton, J. Chiaverini, W. M. Itano, J. D. Jost, C. Langer, and D. J. Wineland, To-

- ward heisenberg-limited spectroscopy with multiparticle entangled states, Science **304**, 1476 (2004).
- [17] M. Auzinsh, D. Budker, D. F. Kimball, S. M. Rochester, J. E. Stalnaker, A. O. Sushkov, and V. V. Yashchuk, Can a quantum nondemolition measurement improve the sensitivity of an atomic magnetometer?, Phys. Rev. Lett. 93, 173002 (2004).
- [18] J. A. Dunningham, Using quantum theory to improve measurement precision, Contemp. Phys. 47, 257 (2006).
- [19] Y. Matsuzaki, S. C. Benjamin, and J. Fitzsimons, Magnetic field sensing beyond the standard quantum limit under the effect of decoherence, Phys. Rev. A 84, 012103 (2011).
- [20] R. Demkowicz-Dobrzański, J. Kołodyński, and M. Guţă, The elusive heisenberg limit in quantum-enhanced metrology, Nature communications 3, 1063 (2012).
- [21] J. G. Bohnet, K. C. Cox, M. A. Norcia, J. M. Weiner, Z. Chen, and J. K. Thompson, Reduced spin measurement back-action for a phase sensitivity ten times beyond the standard quantum limit, Nature Photonics 8, 731 (2014).
- [22] T. Tanaka, P. Knott, Y. Matsuzaki, S. Dooley, H. Yamaguchi, W. J. Munro, and S. Saito, Proposed robust entanglement-based magnetic field sensor beyond the standard quantum limit, Phys. Rev. Lett. 115, 170801 (2015).
- [23] S. Dooley, E. Yukawa, Y. Matsuzaki, G. C. Knee, W. J. Munro, and K. Nemoto, A hybrid-systems approach to spin squeezing using a highly dissipative ancillary system, New Journal of Physics 18, 053011 (2016).
- [24] E. Davis, G. Bentsen, and M. Schleier-Smith, Approaching the heisenberg limit without single-particle detection, Phys. Rev. Lett. 116, 053601 (2016).
- [25] Y. Matsuzaki, S. Benjamin, S. Nakayama, S. Saito, and W. J. Munro, Quantum metrology beyond the classical limit under the effect of dephasing, Phys. Rev. Lett. 120, 140501 (2018).
- [26] W. Happer and H. Tang, Spin-exchange shift and narrowing of magnetic resonance lines in optically pumped alkali vapors, Phys. Rev. Lett. 31, 273 (1973).
- [27] J. C. Allred, R. N. Lyman, T. W. Kornack, and M. V. Romalis, High-sensitivity atomic magnetometer unaffected by spinexchange relaxation, Phys. Rev. Lett. 89, 130801 (2002).
- [28] H. Dang, A. C. Maloof, and M. V. Romalis, Ultrahigh sensitivity magnetic field and magnetization measurements with an atomic magnetometer, Applied Physics Letters 97 (2010).
- [29] M. Bal, C. Deng, J.-L. Orgiazzi, F. Ong, and A. Lupascu, Ultrasensitive magnetic field detection using a single artificial atom, Nature communications 3, 1324 (2012).

- [30] H. Toida, Y. Matsuzaki, K. Kakuyanagi, X. Zhu, W. J. Munro, H. Yamaguchi, and S. Saito, Electron paramagnetic resonance spectroscopy using a single artificial atom, Commun. Phys. 2, 1 (2019).
- [31] V. M. Acosta, E. Bauch, M. P. Ledbetter, C. Santori, K.-M. C. Fu, P. E. Barclay, R. G. Beausoleil, H. Linget, J. F. Roch, F. Treussart, S. Chemerisov, W. Gawlik, and D. Budker, Diamonds with a high density of nitrogen-vacancy centers for magnetometry applications, Phys. Rev. B 80, 115202 (2009).
- [32] G. Balasubramanian, P. Neumann, D. Twitchen, M. Markham, R. Kolesov, N. Mizuochi, J. Isoya, J. Achard, J. Beck, J. Tissler, et al., Ultralong spin coherence time in isotopically engineered diamond, Nature materials 8, 383 (2009).
- [33] F. Dolde, H. Fedder, M. W. Doherty, T. Nöbauer, F. Rempp, G. Balasubramanian, T. Wolf, F. Reinhard, L. C. Hollenberg, F. Jelezko, et al., Electric-field sensing using single diamond spins, Nature Physics 7, 459 (2011).
- [34] T. Ishikawa, K.-M. C. Fu, C. Santori, V. M. Acosta, R. G. Beau-soleil, H. Watanabe, S. Shikata, and K. M. Itoh, Optical and spin coherence properties of nitrogen-vacancy centers placed in a 100 nm thick isotopically purified diamond layer, Nano letters 12, 2083 (2012).
- [35] G. M. Palma, K.-A. Suominen, and A. Ekert, Quantum computers and dissipation, Proceedings of the Royal Society of London. Series A: Mathematical, Physical and Engineering Sciences 452, 567 (1996).
- [36] A. Smirne, J. Kołodyński, S. F. Huelga, and R. Demkowicz-Dobrzański, Ultimate precision limits for noisy frequency estimation, Phys. Rev. Lett. 116, 120801 (2016).
- [37] K. Macieszczak, Zeno limit in frequency estimation with nonmarkovian environments, Phys. Rev. A 92, 010102 (2015).
- [38] W. H. Zurek, Decoherence and the transition from quantum to classical, Physics today 44, 36 (1991).
- [39] H.-P. Breuer and F. Petruccione,
 The theory of open quantum systems
 Press, USA, 2002).

 University
- [40] B. Tratzmiller, Q. Chen, I. Schwartz, S. F. Huelga, and M. B. Plenio, Limited-control metrology approaching the heisenberg limit without entanglement preparation, Physical Review A 101, 032347 (2020).
- [41] Y. Matsuzaki, S. C. Benjamin, and J. Fitzsimons, Magnetic field sensing beyond the standard quantum limit under the effect of decoherence, Physical Review A—Atomic, Molecular, and Optical Physics 84, 012103 (2011).
- [42] E. Schrödinger, Die gegenwärtige situation in der quantenmechanik, Sci. Nat. 23, 823 (1935).
- [43] D. M. Greenberger, M. A. Horne, A. Shimony, and A. Zeilinger, Bell's theorem without inequalities, American Journal of Physics 58, 1131 (1990).
- [44] T. Monz, P. Schindler, J. T. Barreiro, M. Chwalla, D. Nigg, W. A. Coish, M. Harlander, W. Hänsel, M. Hennrich, and R. Blatt, 14-qubit entanglement: Creation and coherence, Phys. Rev. Lett. 106, 130506 (2011).
- [45] L. DiCarlo, M. D. Reed, L. Sun, B. R. Johnson, J. M. Chow, J. M. Gambetta, L. Frunzio, S. M. Girvin, M. H. Devoret, and R. J. Schoelkopf, Preparation and measurement of threequbit entanglement in a superconducting circuit, Nature 467, 574 (2010).
- [46] F. Fröwis, P. Sekatski, W. Dür, N. Gisin, and N. Sangouard, Macroscopic quantum states: Measures, fragility, and implementations, Rev. Mod. Phys. 90, 025004 (2018).
- [47] A. Shimizu and T. Morimae, Detection of macroscopic entanglement by correlation of local observables, Phys. Rev. Lett. 95, 090401 (2005).

- [48] We use the notation $\Theta(N^k)$ in addition to the standard notation $O(N^k)$, i.e., $O(N^k)/N^k \to \mathrm{const.} (\neq 0)$ in the limit $N \to \infty$, as the following meaning: For a function g of N, we say $g = \Theta(N^k)$ if g/N^k approaches a positive constant as $N \to \infty$. If $g = \Theta(N^k)$ then $g = O(N^k)$, but the inverse is not necessarily true
- [49] S. F. Huelga, C. Macchiavello, T. Pellizzari, A. K. Ekert, M. B. Plenio, and J. I. Cirac, Improvement of frequency standards with quantum entanglement, Phys. Rev. Lett. 79, 3865 (1997).
- [50] M. Tatsuta and A. Shimizu, Conversion of thermal equilibrium states into superpositions of macroscopically distinct states, Phys. Rev. A 97, 012124 (2018).
- [51] A. Shimizu and T. Morimae, Detection of macroscopic entanglement by correlation of local observables, Phys. Rev. Lett. 95, 090401 (2005).
- [52] M. Tatsuta, Y. Matsuzaki, and A. Shimizu, Quantum metrology with generalized cat states, Phys. Rev. A 100, 032318 (2019).
- [53] Note that $\hat{a}(l)$ is allowed to be different from the spatial translation of $\hat{a}(l')$ ($l' \neq l$), i.e., \hat{A} may not be translation invariant.
- [54] J. Liu, H. Yuan, X.-M. Lu, and X. Wang, Quantum fisher information matrix and multiparameter estimation, Journal of Physics A: Mathematical and Theoretical 53, 023001 (2020).
- [55] A. M. Tyryshkin, S. Tojo, J. J. Morton, H. Riemann, N. V. Abrosimov, P. Becker, H.-J. Pohl, T. Schenkel, M. L. Thewalt, K. M. Itoh, et al., Electron spin coherence exceeding seconds in high-purity silicon, Nature materials 11, 143 (2012).
- [56] This preparation is possible by, for example, just waiting a long time that is longer than the thermal relaxation time, which is much longer than the coherence time.
- [57] I. Chiorescu, Y. Nakamura, C. M. Harmans, and J. Mooij, Coherent quantum dynamics of a superconducting flux qubit, Science 299, 1869 (2003).
- [58] A. Lupaşcu, C. Verwijs, R. Schouten, C. Harmans, and J. Mooij, Nondestructive readout for a superconducting flux qubit, Phys. Rev. Lett. 93, 177006 (2004).
- [59] I. Chiorescu, P. Bertet, K. Semba, Y. Nakamura, C. Harmans, and J. Mooij, Coherent dynamics of a flux qubit coupled to a harmonic oscillator, Nature 431, 159 (2004).
- [60] J. Majer, F. Paauw, A. Ter Haar, C. Harmans, and J. Mooij, Spectroscopy on two coupled superconducting flux qubits, Phys. Rev. Lett. 94, 090501 (2005).
- [61] F. Paauw, A. Fedorov, C. M. Harmans, and J. Mooij, Tuning the gap of a superconducting flux qubit, Phys. Rev. Lett. 102, 090501 (2009).
- [62] X. Zhu, A. Kemp, S. Saito, and K. Semba, Coherent operation of a gap-tunable flux qubit, Applied Physics Letters 97 (2010).
- [63] N. Lambert, Y. Matsuzaki, K. Kakuyanagi, N. Ishida, S. Saito, and F. Nori, Superradiance with an ensemble of superconducting flux qubits, Phys. Rev. B 94, 224510 (2016).
- [64] T. Tanaka, P. Knott, Y. Matsuzaki, S. Dooley, H. Yamaguchi, W. J. Munro, and S. Saito, Proposed robust entanglement-based magnetic field sensor beyond the standard quantum limit, Phys. Rev. Lett. 115, 170801 (2015).
- [65] H. Toida, Y. Matsuzaki, K. Kakuyanagi, X. Zhu, W. J. Munro, H. Yamaguchi, and S. Saito, Electron paramagnetic resonance spectroscopy using a single artificial atom, Communications Physics 2, 33 (2019).
- [66] K. Miyanishi, Y. Matsuzaki, H. Toida, K. Kakuyanagi, M. Negoro, M. Kitagawa, and S. Saito, Architecture to achieve nuclear magnetic resonance spectroscopy with a superconducting flux qubit, Phys. Rev. A 101, 052303 (2020).
- [67] R. P. Budoyo, K. Kakuyanagi, H. Toida, Y. Matsuzaki, and S. Saito, Electron spin resonance with up to 20 spin sensitivity

- measured using a superconducting flux qubit, Applied Physics Letters **116** (2020).
- [68] J. Bylander, S. Gustavsson, F. Yan, F. Yoshihara, K. Harrabi, G. Fitch, D. G. Cory, Y. Nakamura, J.-S. Tsai, and W. D. Oliver, Noise spectroscopy through dynamical decoupling with a superconducting flux qubit, Nature Physics 7, 565 (2011).
- [69] A. Lupaşcu, S. Saito, T. Picot, P. De Groot, C. Harmans, and J. Mooij, Quantum non-demolition measurement of a superconducting two-level system, nature physics 3, 119 (2007).
- [70] Z. Lin, K. Inomata, W. Oliver, K. Koshino, Y. Nakamura, J. Tsai, and T. Yamamoto, Single-shot readout of a superconducting flux qubit with a flux-driven josephson parametric amplifier, Applied Physics Letters 103 (2013).
- [71] D. Marcos, M. Wubs, J. Taylor, R. Aguado, M. D. Lukin, and A. S. Sørensen, Coupling nitrogen-vacancy centers in diamond to superconducting flux qubits, Phys. Rev. Lett. 105, 210501 (2010).
- [72] J. Twamley and S. D. Barrett, Superconducting cavity bus for single nitrogen-vacancy defect centers in diamond, Phys. Rev. B—Condensed Matter and Materials Physics 81, 241202 (2010).
- [73] X. Zhu, S. Saito, A. Kemp, K. Kakuyanagi, S.-i. Karimoto, H. Nakano, W. J. Munro, Y. Tokura, M. S. Everitt, K. Nemoto, et al., Coherent coupling of a superconducting flux qubit to an electron spin ensemble in diamond, Nature 478, 221 (2011).
- [74] S. Saito, X. Zhu, R. Amsüss, Y. Matsuzaki, K. Kakuyanagi, T. Shimo-Oka, N. Mizuochi, K. Nemoto, W. J. Munro, and K. Semba, Towards realizing a quantum memory for a superconducting qubit: Storage and retrieval of quantum states, Phys. Rev. Lett. 111, 107008 (2013).

- [75] X. Zhu, Y. Matsuzaki, R. Amsüss, K. Kakuyanagi, T. Shimo-Oka, N. Mizuochi, K. Nemoto, K. Semba, W. J. Munro, and S. Saito, Observation of dark states in a superconductor diamond quantum hybrid system, Nature communications 5, 3524 (2014).
- [76] H. Nakazato, T. Takazawa, and K. Yuasa, Purification through zeno-like measurements, Physical review letters 90, 060401 (2003).
- [77] J. K. Stockton, R. Van Handel, and H. Mabuchi, Deterministic dicke-state preparation with continuous measurement and control, Phys. Rev. A 70, 022106 (2004).
- [78] D. B. R. Dasari, S. Yang, A. Chakrabarti, A. Finkler, G. Kurizki, and J. Wrachtrup, Anti-zeno purification of spin baths by quantum probe measurements, Nature communications 13, 7527 (2022).
- [79] R. H. Dicke, Coherence in spontaneous radiation processes, Physical review 93, 99 (1954).
- [80] J. K. Stockton, J. Geremia, A. C. Doherty, and H. Mabuchi, Characterizing the entanglement of symmetric many-particle spin-1 2 systems, Phys. Rev. A 67, 022112 (2003).
- [81] N. Kiesel, W. Wieczorek, S. Krins, T. Bastin, H. Weinfurter, and E. Solano, Operational multipartite entanglement classes for symmetric photonic qubit states, Phys. Rev. A 81, 032316 (2010).
- [82] T. Benoist, M. Fraas, Y. Pautrat, and C. Pellegrini, Invariant measure for quantum trajectories, Probability Theory and Related Fields 174, 307 (2019).
- [83] K. Mochizuki and R. Hamazaki, Measurement-induced spectral transition, Phys. Rev. Lett. 134, 010410 (2025).